AUTOMATIC MASS BALANCING SYSTEM FOR THE 5-DOF SPACECRAFT SIMULATOR

A Thesis
Presented to
The Academic Faculty

by

Su Yeon Choi

In Partial Fulfillment
of the Requirements for the Degree
Master of Science in the
Daniel Guggenheim School of Aerospace Engineering

Georgia Institute of Technology
August 2016

AUTOMATIC MASS BALANCING SYSTEM FOR THE 5-DOF SPACECRAFT SIMULATOR

Approved by:

Professor Panagiotis Tsiotras, Advisor
Daniel Guggenheim School of Aerospace Engineering
Georgia Institute of Technology

Professor Marcus Holzinger
Daniel Guggenheim School of Aerospace Engineering
Georgia Institute of Technology

Professor Mark Costello
Daniel Guggenheim School of Aerospace Engineering
Georgia Institute of Technology

Date Approved: July 18 2016

To my family

ACKNOWLEDGEMENTS

First and foremost, I would like to express my sincere gratitude to my advisor, Prof. Panagiotis Tsiotras for giving me the opportunity to join his group, for his motivation, advice, and patience since then.

I would also like to express my gratitude to my advisory committee members, Prof. Marcus Holzinger and Prof. Mark Costello to provide valuable time and advice.

Further, I would also like to thank Republic of Korea Army for giving me the chance to study at Georgia Tech and for continuous financial support and encouragement.

I would also like to thank the members of the Dynamics and Control Systems Laboratory. Especially, I am grateful to Alfredo Valverde, who was always willing to help me. This research would not be possible without his support and friendship.

Finally, I would like to thank my family and friends for encouraging me spiritually throughout writing this thesis and my life.

TABLE OF CONTENTS

LIST OF TABLES

LIST OF FIGURES

SUMMARY

Spacecraft simulators are widely used to validate spacecraft attitude determination and control techniques. The Autonomous Spacecraft Testing of Robotic Operations in Space (ASTROS) facility at the School of Aerospace Engineering at the Georgia Institute of Technology has been developed to create spacelike environment for academic research and education. This facility is composed of two stages: The upper stage has a hemi-spherical air-bearing that allows frictionless rotational motion of the upper stage, and the lower stage has three linear air-bearing pads that make it possible to achieve almost friction-free translational motion of the entire system. Therefore, these two types of air-bearings enable the platform to have five degrees of freedom in order to test both attitude and position controlling problems.

In this system, the balancing procedure is a crucial issue that will minimize gravitational torques acting on the spacecraft simulator. This work introduces an automatic mass balancing method and eliminates the center of gravity offset from the center of rotation by actuating three sliding masses. First, PID attitude feedback controller is proposed to balance x and y directions. Second, an Extended Kalman Filter is introduced to estimate the vertical imbalance since the linear actuators cannot control the vertical direction by sliding masses. Finally, the proposed controller and the EKF are tested on the simulation and the ASTROS facility. The quaternions are measured from a dual-axis inclinometer and the angular velocities are calculated from derivatives of the quaternions during the experiments.

CHAPTER I

INTRODUCTION

1.1 General Introduction

Experimental facilities for testing spacecraft dynamics are imperative to reduce various risks and costs. Since 2000, the Dynamics and Control Systems Laboratory at the School of Aerospace Engineering at Georgia Tech has established several air-bearing-based spacecraft platforms. Similar facilities in other laboratories use air-bearing systems to achieve frictionless sliding over a smooth surface. Historical review of air-bearing spacecraft simulators is presented in Ref. [19].

The ground-based spacecraft simulator needs to create a frictionless and torque-free environment. However, there are various disturbance elements acting on the platform. These elements are categorized into four groups [21]: torques arising from the platform, air-bearings, environment, and system. The major disturbance torque is from the gravity due to a shift of the center of mass from the center of rotation in the spherical air-bearing-based simulators. To minimize this gravitational torque, the center of mass of the system needs to be aligned with the center of rotation. In other words, the simulator must be balanced. A manual procedure to minimize the offset between the center of mass and the center of rotation is presented in Ref. [5]. Fullmer states that the most effective method for manual balancing is to balance two horizontal axes by first moving balance masses, and raising the vertical mass by inspecting the pendulum motion of the system until the oscillatory period becomes effectively long. However, the manual method requires considerable amount of time and skill and does not guarantee the accurate estimation of the center of mass.

The aim of this study is to propose an automatic mass balancing system in order

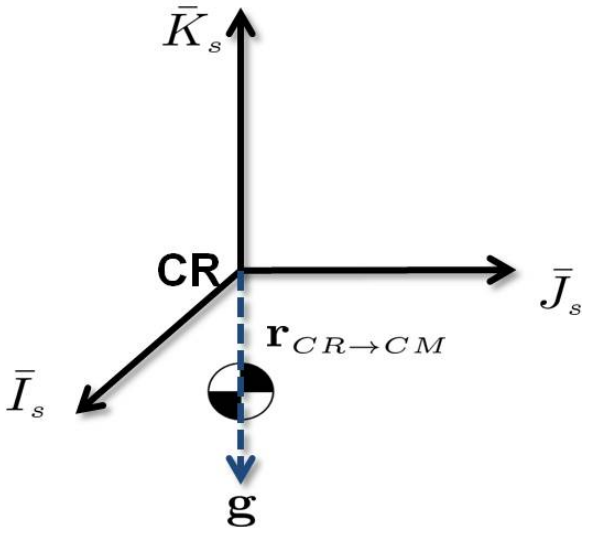

Figure 1: Offset vector along the gravity

to overcome the difficulties of the manual system. Many spacecraft simulators have been equipped with automatic balancing systems [1, 7, 10, 16, 17, 24]. Automatic mass balancing systems with three proof masses for compensation of unbalance were proposed in Refs. [1, 10]. External control moment gyros were used to track the angular momentum and to determine the positions of proof masses [10]. Three electric motors were proposed to move sliding masses along three axes [1].

A batch estimation technique was introduced in order to calculate the mass moment of inertia and the center of gravity [8], where a least-squares estimation was used to determine unknown parameters. Various estimation methods are presented in Refs. [1, 10, 11, 15, 18, 22]. This study proposes an inertia-free attitude controller, which does not require a priori knowledge of the mass identification. However, the proposed control law cannot compensate the offset component along the vertical axis as shown in Fig. 1. To overcome this challenge, Extended Kalman Filter is used to estimate the offset along the gravity field and slowly move to the center of mass by sliding the balance mass with a small velocity in the last direction.

The proposed work aims at designing the controller, validating it through the

simulation using MATLAB/Simulink, and implementing the system to the ASTROS facility.

1.2 5-DOF Experimental Platform

For this study, a 5-DOF experimental platform of the ASTROS facility is introduced to simulate autonomous rendezvous and docking (ARD) and other general proximity operations [2,23]. The platform includes an upper stage supported on a hemispherical air bearing and a lower stage consisting of three linear air-bearing pads. Therefore, two types of air-bearings enable the platform to achieve almost friction-free translational/rotational motion of the system over a flat epoxy floor. More details about ASTROS facility and its 5-DOF platform can be found in Refs. [2, 8, 23]. Pictures of the platform and its manual balancing system are shown in Fig. 2.

The upper stage is equipped with 12 cold-gas thrusters for attitude and translational controls, each thruster providing a maximum of 5 N force. A thruster allocation algorithm was developed to distribute required forces and moments to the thrusters [2]. The four Variable-Speed Control Moment Gyros (VSCMGs) are arranged in a conventional pyramid configuration on the platform to provide moments for fine attitude control. Therefore, the control moments can be allocated to the thrusters and/or the VSCMGs, while the control force can only be actuated by the thrusters. The on-board attitude sensors include an inertial measurement unit (IMU), a two-axis Sun/star sensor, a three-axis magnetometer, a three-axis rate gyro (RG02-3201 by Humphrey), and a two-axis inclinometer. A VICON motion capture system has been installed on the experimental arena to provide accurate localization and attitude information with respect to an inertial frame [23].

All air-bearings are manually operated via external switches, and all sensors, the thrusters, and the VSCMGs are remotely controlled by the on-board computer, which

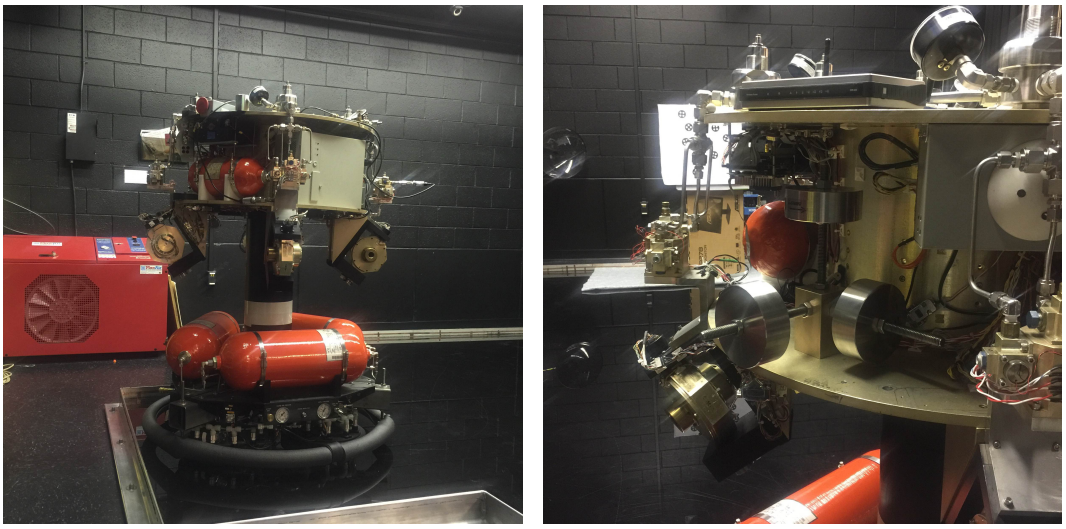

Figure 2: The 5-DOF experimental platform and the manual balancing system

runs Mathworks' xPC Target real-time environment. There are three different operation modes, which allow one to selectively open and close the valves for a 3-DOF translational/rotational mode with heading change (only lower platform levitated), full 3-DOF rotational mode (only upper platform levitated), and full 5-DOF translational/rotational mode (both upper and lower platforms levitated). This provides great flexibility for the type of experiments one may conduct using the ASTROS.

1.3 Research Objectives

The overall objective of this work is to design a inertia-free adaptive attitude tracking controller in order to relocate the platform's center of mass toward the geometrical center of the spherical air-bearing, and implement the design in the spacecraft simulator. The specific objectives of the thesis are summarized below.

- Study on the system dynamic model and the PID attitude control
  - Model the spacecraft simulator kinematics and dynamics
  - Design a PID attitude controller for the balancing system
  - Estimate attitude and an unknown parameter (distance between the center

of gravity and the center of rotation) using an extended Kalman filter

- Implementation of the controller through the simulation and the experiment
  - Validate the system through the simulation using MATLAB/Simulink model
  - Validate the system experimentally on the ASTROS facility

CHAPTER II

DERIVATION OF THE EQUATIONS OF MOTION OF THE PLATFORM

2.1 Nomenclature

$\mathbf{a}_{x/y}$ acceleration of point x with respect to the y-frame

$\boldsymbol{\alpha}_{x/y}$ angular acceleration of body x with respect to the y-frame

$\Large\clubsuit_{*}$ Center of mass of $*$

$_{CR}$ Center of rotation of the platform

$\delta\mathbf{r}_{M\rightarrow m_j}$ Displacement of the balance masses

$_{F}$ Bus of the upper stage of the platform (does not include gimbals, wheels and the proof masses)

$\mathbf{g}^{s}$ Gravity vector expressed in S-frame

$^{x}\mathbf{I}_{y}$ mass moment of inertia of body y about the point x

$\boldsymbol{\omega}_{x/y}$ Angular velocity vector of body x with respect to the y-frame

m_{*} Mass of body *

$\mathbf{r}_{x\rightarrow y}$ Translation vector from point x to point y

$_{S}$ Upper stage with gimbals and wheels(does not include the proof masses)

$_{U}$ Upper stage with gimbals, wheels and proof masses

$\mathbf{q}_{x/y}$ quaternion vector that represents the pose of X-frame with respect to the Y-frame

2.2 Reference Frames

- Intertial reference frame (I-frame) : reference frame with origin at the fixed point of the epoxy floor.

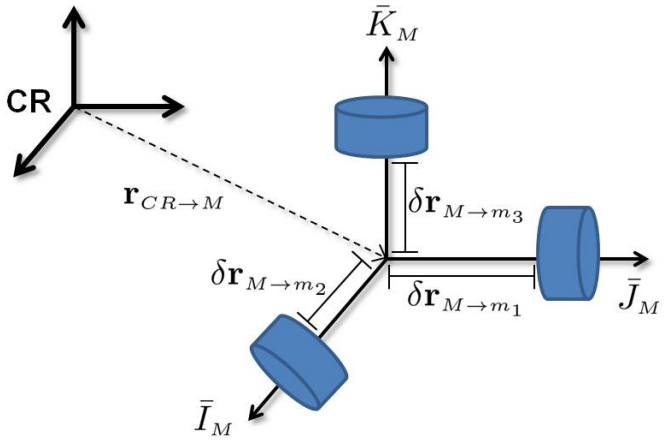

Figure 3: Definition of the M-frame with respect to the proof masses

- Upper stage reference frame (S-frame) : reference frame of the body S (the upper stage with the gimbals and wheels but without the proof masses) with origin at the center of rotation.

- Upper stage bus reference frame (F-frame) : reference frame of body F (upper stage without the gimbals, wheels and proof masses) with origin at the center of the upper stage bus.

- Proof masses reference frame (M-frame) : reference frame with $\bar{I}_M$ aligned with the position of a proof mass m_1, $\bar{J}_M$ aligned with m_2, $\bar{K}_M$ aligned with m_3, and origin at the initial location of the balancing masses as shown in Fig. 3.

- Gimbal i reference frame (G_i frame) : reference frame of body G_i (Gimbal i) with origin at the center of mass of gimbal i.

- Wheel i reference frame (W_i frame) : reference frame of body W_i with origin at the center of mass of wheel i.

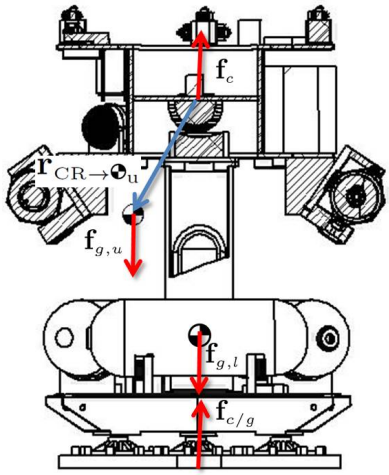

Figure 4: Forces acting on the platform

2.3 Equations of motion of the Upper Stage

From classical Newton/Euler dynamics, the translational dynamic equations of motion of the center of mass of the upper stage are given by

$$m_s \mathbf{a}_{\bullet_u/I} = \mathbf{f}_{g,u} + \mathbf{f}_c \tag{1}$$

where $\mathbf{f}_{g,u}$ is the gravitational force acting on the upper stage and $\mathbf{f}_c$ is the contact force acting on the upper stage due to the lower stage as shown in Fig. 4. The acceleration of the center of mass of the upper stage with respect to the inertial frame can be rewritten in terms of the acceleration of the center of rotation with respect to the inertial frame as follows

$$\mathbf{r}_{O\to\bullet_u} = \mathbf{r}_{O\to CR} + \mathbf{r}_{CR\to\bullet_u} \tag{2}$$

The inertial frame time derivative of this expression is given by

$$\frac{{}^I\mathrm{d}}{\mathrm{dt}}\mathbf{r}_{O\to\bullet_u} = \frac{{}^I\mathrm{d}}{\mathrm{dt}}\mathbf{r}_{O\to CR} + \frac{{}^I\mathrm{d}}{\mathrm{dt}}\mathbf{r}_{CR\to\bullet_u} \tag{3}$$

$$\mathbf{v}_{\bullet_u/I} = \mathbf{v}_{CR/I} + \mathbf{v}_{\bullet_u/S} + \boldsymbol{\omega}_{S/I} \times \mathbf{r}_{CR\to\bullet_u} \tag{4}$$

Take an I-frame derivative of this equation.

$$\frac{{}^{I}\mathrm{d}}{\mathrm{dt}}\mathbf{v}_{\bullet_u/I} = \frac{{}^{I}\mathrm{d}}{\mathrm{dt}}\mathbf{v}_{CR/I} + \frac{{}^{I}\mathrm{d}}{\mathrm{dt}}\mathbf{v}_{\bullet_u/S} + \frac{{}^{I}\mathrm{d}}{\mathrm{dt}}\left(\boldsymbol{\omega}_{S/I} \times \mathbf{r}_{CR\to\bullet_u}\right) \tag{5}$$

$$\mathbf{a}_{\bullet_u/I} = \mathbf{a}_{CR/I} + \mathbf{a}_{\bullet_u/S} + \boldsymbol{\alpha}_{S/I} \times \mathbf{r}_{CR\to\bullet_u} + 2\left(\boldsymbol{\omega}_{S/I} \times \mathbf{v}_{\bullet_u/S}\right) + \boldsymbol{\omega}_{S/I} \times \left(\boldsymbol{\omega}_{S/I} \times \mathbf{r}_{CR\to\bullet_u}\right) \tag{6}$$

Then, the translational equation of motion of the upper stage is rewritten by noting that $\mathbf{r}_{CR\to\bullet_u} = \frac{1}{m_u}\left(m_s\mathbf{r}_{CR\to\bullet_s} + \sum_{j=1}^{3} m_j\delta\mathbf{r}_{M\to m_j}\right)$. This yields

$$\begin{aligned} &m_u\mathbf{a}_{CR/I} + m_s\left(\mathbf{a}_{\bullet_s/S} + \boldsymbol{\alpha}_{S/I} \times \mathbf{r}_{CR\to\bullet_s} + 2\left(\boldsymbol{\omega}_{S/I} \times \mathbf{v}_{\bullet_s/S}\right) + \boldsymbol{\omega}_{S/I} \times \left(\boldsymbol{\omega}_{S/I} \times \mathbf{r}_{CR\to\bullet_s}\right)\right) \\ &+ \sum_{j=1}^{3} m_j\left(\mathbf{a}_{m_j/S} + \boldsymbol{\alpha}_{S/I} \times \delta\mathbf{r}_{M\to m_j} + 2\left(\boldsymbol{\omega}_{S/I} \times \mathbf{v}_{m_j/S}\right) + \boldsymbol{\omega}_{S/I} \times \left(\boldsymbol{\omega}_{S/I} \times \delta\mathbf{r}_{M\to m_j}\right)\right) = \mathbf{f}_{g,u} + \mathbf{f}_c \end{aligned} \tag{7}$$

The rotational dynamic equations of motion of the system composed by the upper stage bus, the gimbals and wheels of the VSCMGs, and the proof masses are given by

$$\frac{{}^{I}\mathrm{d}}{\mathrm{dt}}{}^{CR}\mathbf{H}_{u/I} + \mathbf{r}_{CR\to\bullet_u} \times m_u\mathbf{a}_{CR/I} = \mathbf{r}_{CR\to\bullet_u} \times \mathbf{f}_{g,u} + {}^{CR}\boldsymbol{\tau}_c \tag{8}$$

where ${}^{CR}\boldsymbol{\tau}_c$ is the contact moment vector on the upper stage due to the lower stage about point CR. Note that ${}^{CR}\boldsymbol{\tau}_c$ is assumed to be zero in the 3-DOF and 5-DOF case. ${}^{CR}\mathbf{H}_{u/I}$ can be calculated as follows

$$\begin{aligned} {}^{CR}\mathbf{H}_{u/I} =& {}^{CR}\mathbf{I}_u\boldsymbol{\omega}_{S/I} + {}^{\bullet_f}\mathbf{I}_f\boldsymbol{\omega}_{F/S} + \sum_{i=1}^{4} {}^{\bullet_{W_i}}\mathbf{I}_{W_i}\boldsymbol{\omega}_{W_i/S} + \sum_{i=1}^{4} {}^{\bullet_{G_i}}\mathbf{I}_{G_i}\boldsymbol{\omega}_{G_i/S} + \sum_{j=1}^{3} {}^{m_j}\mathbf{I}_{m_j}\boldsymbol{\omega}_{m_j/S} \\ &+ m_f\mathbf{r}_{CR\to\bullet_f} \times \mathbf{v}_{\bullet_f/S} + \sum_{i=1}^{4} m_{W_i}\mathbf{r}_{CR\to\bullet_{W_i}} \times \mathbf{v}_{\bullet_{W_i}/S} + \sum_{i=1}^{4} m_{G_i}\mathbf{r}_{CR\to\bullet_{G_i}} \times \mathbf{v}_{\bullet_{G_i}/S} \\ &+ \sum_{j=1}^{3} m_j\delta\mathbf{r}_{M\to m_j} \times \mathbf{v}_{m_j/S} \end{aligned} \tag{9}$$

This equation can be simplified by noting that $\boldsymbol{\omega}_{F/S} = \boldsymbol{\omega}_{m_j/S} = 0$ and $\boldsymbol{\omega}_{W_i/S} = \boldsymbol{\omega}_{W_i/Gi} + \boldsymbol{\omega}_{G_i/S}$ and assuming that the centers of mass of the gimbals coincide with the centers of mass of the wheels and that the centers of mass of the wheels and of the gimbals do not move with respect to the S-frame which implies $m_f\mathbf{v}_{\bullet_f/S} = m_s\mathbf{v}_{\bullet_s/S}$ and ${}^{\bullet_{C_i}}\mathbf{I}_{C_i} =$

${}^{\bullet_{C_i}}\mathbf{I}_{G_i} + {}^{\bullet_{C_i}}\mathbf{I}_{W_i}$. This yields

$$ {}^{CR}\mathbf{H}_{U/I} = {}^{CR}\mathbf{I}_u\boldsymbol{\omega}_{S/I} + \sum_{i=1}^{4} {}^{\bullet_{C_i}}\mathbf{I}_{W_i}\boldsymbol{\omega}_{W_i/G_i} + \sum_{i=1}^{4} {}^{\bullet_{C_i}}\mathbf{I}_{C_i}\boldsymbol{\omega}_{G_i/S} + m_s\mathbf{r}_{CR\to\bullet_f}\times\mathbf{v}_{\bullet_s/S} + \sum_{j=1}^{3} m_j\delta\mathbf{r}_{M\to m_j}\times\mathbf{v}_{m_j/S} \tag{10} $$

The I-frame time derivative of this equation is given by

$$ \begin{aligned} &\frac{{}^{I}\mathrm{d}}{\mathrm{dt}}{}^{CR}\mathbf{H}_{U/I} = \frac{{}^{S}\mathrm{d}}{\mathrm{dt}}{}^{CR}\mathbf{H}_{U/I} + \boldsymbol{\omega}_{S/I}\times{}^{CR}\mathbf{H}_{U/I} \\ &= \frac{{}^{S}\mathrm{d}}{\mathrm{dt}}{}^{CR}\mathbf{I}_u\boldsymbol{\omega}_{S/I} + {}^{CR}\mathbf{I}_u\boldsymbol{\alpha}_{S/I} + \frac{{}^{S}\mathrm{d}}{\mathrm{dt}}\sum_{i=1}^{4} {}^{\bullet_{C_i}}\mathbf{I}_{W_i}\boldsymbol{\omega}_{W_i/G_i} + \frac{{}^{S}\mathrm{d}}{\mathrm{dt}}\sum_{i=1}^{4} {}^{\bullet_{C_i}}\mathbf{I}_{C_i}\boldsymbol{\omega}_{G_i/S} + m_s\mathbf{r}_{CR\to\bullet_f}\times\mathbf{a}_{\bullet_s/S} \\ &\quad + \boldsymbol{\omega}_{S/I}\times\left({}^{CR}\mathbf{I}_u\boldsymbol{\omega}_{S/I} + \sum_{i=1}^{4} {}^{\bullet_{C_i}}\mathbf{I}_{W_i}\boldsymbol{\omega}_{W_i/G_i} + \sum_{i=1}^{4} {}^{\bullet_{C_i}}\mathbf{I}_{C_i}\boldsymbol{\omega}_{G_i/S} + m_s\mathbf{r}_{CR\to\bullet_f}\times\mathbf{v}_{\bullet_s/S}\right) \\ &\quad + \sum_{j=1}^{3} m_j\delta\mathbf{r}_{M\to m_j}\times\mathbf{a}_{m_j/S} + \boldsymbol{\omega}_{S/I}\times(\sum_{j=1}^{3} m_j\delta\mathbf{r}_{M\to m_j}\times\mathbf{v}_{m_j/S}) \end{aligned} \tag{11} $$

Finally, the rotational equation of motion is written as

$$ \begin{aligned} &\frac{{}^{S}\mathrm{d}}{\mathrm{dt}}{}^{CR}\mathbf{I}_u\boldsymbol{\omega}_{S/I} + {}^{CR}\mathbf{I}_u\boldsymbol{\alpha}_{S/I} + \frac{{}^{S}\mathrm{d}}{\mathrm{dt}}\sum_{i=1}^{4} {}^{\bullet_{C_i}}\mathbf{I}_{W_i}\boldsymbol{\omega}_{W_i/G_i} + \frac{{}^{S}\mathrm{d}}{\mathrm{dt}}\sum_{i=1}^{4} {}^{\bullet_{C_i}}\mathbf{I}_{C_i}\boldsymbol{\omega}_{G_i/S} + m_s\mathbf{r}_{CR\to\bullet_f}\times\mathbf{a}_{\bullet_s/S} \\ &+ \boldsymbol{\omega}_{S/I}\times({}^{CR}\mathbf{I}_u\boldsymbol{\omega}_{S/I} + \sum_{i=1}^{4} {}^{\bullet_{C_i}}\mathbf{I}_{W_i}\boldsymbol{\omega}_{W_i/G_i} + \sum_{i=1}^{4} {}^{\bullet_{C_i}}\mathbf{I}_{C_i}\boldsymbol{\omega}_{G_i/S} + m_s\mathbf{r}_{CR\to\bullet_f}\times\mathbf{v}_{\bullet_s/S}) \\ &+ \sum_{j=1}^{3} m_j\delta\mathbf{r}_{M\to m_j}\times\mathbf{a}_{m_j/S} + \boldsymbol{\omega}_{S/I}\times(\sum_{j=1}^{3} m_j\delta\mathbf{r}_{M\to m_j}\times\mathbf{v}_{m_j/S}) + \mathbf{r}_{CR\to\bullet_u}\times m_u\mathbf{a}_{CR/I} \\ &= \mathbf{r}_{CR\to\bullet_u}\times\mathbf{f}_{g,u} \end{aligned} \tag{12} $$

2.4 Equations of Motion for the 3-DOF case

In this case, the equations of motion only describe the rotation of the upper stage since the lower stage is fixed with respect to the inertial frame during auto-balancing ($\mathbf{a}_{CR/I} = 0$). Moreover, $\boldsymbol{\omega}_{Wi/Gi} = \boldsymbol{\omega}_{Gi/S} = 0$ because VSCMGs are not used for the balancing system. Therefore, the rotational equations of motion from Eq. (12) can

be written as

$$\begin{aligned}&\frac{{}^{S}\mathrm{d}}{\mathrm{dt}}{}^{CR}\mathbf{I}_{u}\boldsymbol{\omega}_{S/I}+{}^{CR}\mathbf{I}_{u}\boldsymbol{\alpha}_{S/I}+\sum_{j=1}^{3}m_{j}\delta\mathbf{r}_{M\to m_{j}}\times\mathbf{a}_{m_{j}/S}\\&+\boldsymbol{\omega}_{S/I}\times\left({}^{CR}\mathbf{I}_{u}\boldsymbol{\omega}_{S/I}+\sum_{j=1}^{3}m_{j}\delta\mathbf{r}_{M\to m_{j}}\times\mathbf{v}_{m_{j}/S}\right)=\mathbf{r}_{CR\to\bullet_{u}}\times\mathbf{f}_{g,u}\end{aligned}\tag{13}$$

Note that the mass moment of inertia of the upper stage can be calculated as

$${}^{CR}\mathbf{I}_{u}={}^{CR}\mathbf{I}_{s}-\sum_{j=1}^{3}m_{j}\left[\delta\mathbf{r}_{M\to m_{j}}\times\right]\left[\delta\mathbf{r}_{M\to m_{j}}\times\right]$$

$$\text{where }\left[\delta\mathbf{r}_{M\to m_{j}}\times\right]=\begin{bmatrix}0&-r_{3}&r_{2}\\r_{3}&0&-r_{1}\\-r_{2}&r_{1}&0\end{bmatrix},\ \delta\mathbf{r}_{M\to m_{j}}=\begin{bmatrix}r_{1}\\r_{2}\\r_{3}\end{bmatrix}$$

The S-frame time derivative of mass moment of inertia of the upper stage can be written as

$$\frac{{}^{S}\mathrm{d}{}^{CR}\mathbf{I}_{u}}{\mathrm{dt}}=\sum_{j=1}^{3}\frac{{}^{S}\mathrm{d}{}^{CR}\mathbf{I}_{m_{j}}}{\mathrm{dt}}$$

$$=2\begin{bmatrix}m_{2}v_{22}r_{22}+m_{3}v_{33}r_{33}&0&0\\0&m_{1}v_{11}r_{11}+m_{3}v_{33}r_{33}&0\\0&0&m_{1}v_{11}r_{11}+m_{2}v_{22}r_{22}\end{bmatrix}$$

where

$$\delta\mathbf{r}_{M\to m_{1}}=\begin{bmatrix}r_{11}\\0\\0\end{bmatrix},\ \mathbf{v}_{m_{1}/S}=\begin{bmatrix}v_{11}\\0\\0\end{bmatrix},\ \delta\mathbf{r}_{M\to m_{2}}=\begin{bmatrix}0\\r_{22}\\0\end{bmatrix},\tag{14}$$

$$\mathbf{v}_{m_{2}/S}=\begin{bmatrix}0\\v_{22}\\0\end{bmatrix},\ \delta\mathbf{r}_{M\to m_{3}}=\begin{bmatrix}0\\0\\r_{33}\end{bmatrix},\ \mathbf{v}_{m_{3}/S}=\begin{bmatrix}0\\0\\v_{33}\end{bmatrix}$$

The time derivative of the mass moment of inertia is greatly small, so that this term is neglected in the system dynamic model of the balancing system. The center of

mass of the upper stage is calculated as

$$\mathbf{r}_{CR\to\bullet_u} = \frac{1}{m_u}\left(m_s\mathbf{r}_{CR\to\bullet_s} + \sum_{j=1}^{3} m_j \delta\mathbf{r}_{M\to m_j}\right) \tag{15}$$

where $\mathbf{r}_{CR\to\bullet_u}$ is the position vector from the center of rotation to the center of mass of the upper stage.

2.5 Kinematics

The rotational kinematics using a quaternion is given by

$$\begin{bmatrix}\dot{q}_1\\ \dot{q}_2\\ \dot{q}_3\\ \dot{q}_4\end{bmatrix} = \frac{1}{2}\begin{bmatrix}0 & -\omega_x & -\omega_y & -\omega_z\\ \omega_x & 0 & \omega_z & -\omega_y\\ \omega_y & -\omega_z & 0 & \omega_x\\ \omega_z & \omega_y & -\omega_x & 0\end{bmatrix}\begin{bmatrix}q_1\\ q_2\\ q_3\\ q_4\end{bmatrix}, \text{ where } \boldsymbol{\omega}_{S/I} = \begin{bmatrix}\omega_x\\ \omega_y\\ \omega_z\end{bmatrix} \text{ and } \mathbf{q}_{S/I} = \begin{bmatrix}q_1\\ q_2\\ q_3\\ q_4\end{bmatrix} \tag{16}$$

In summary, the dynamics and the kinematics for the balancing system are calculated from Eq. (13) and Eq. (16).

CHAPTER III

THE PID CONTROLLER AND THE EXTENDED KALMAN FILTER FOR ESTIMATION

3.1 PID Controller

As mentioned before, the automatic balancing system is crucial to minimizing disturbance torques on the simulator. In this section, a PID control technique is used to compensate for the center of gravity offset. The main idea of the balancing system is to move three proof masses in order to relocate the center of mass until it coincides with the geometric center of rotation. In other words, when the spacecraft simulator is perfectly balanced and the angular momentum is conserved, the distance between the center of rotation and the center of mass is zero. The rotational equation of motion can be simplified due to negligibly small velocities and accelerations of the balancing masses. As shown in Fig. 5, angular acceleration errors ($\boldsymbol{\alpha}_{S/I}^{err}$) between Eq. (13) and the simplified dynamic model below are less than $10^{-10}\, rad/s^2$, which can be ignored. Therefore, the system dynamics from Eq. (13) can be simplified as

$$ {}^{CR}\mathbf{I}_u \boldsymbol{\alpha}_{S/I} + \boldsymbol{\omega}_{S/I} \times {}^{CR}\mathbf{I}_u \boldsymbol{\omega}_{S/I} = \mathbf{r}_{CR\to \bullet_u} \times \mathbf{f}_{g,u} + \boldsymbol{\tau} \tag{17} $$

where $\boldsymbol{\tau}$ is the control torque generated by sliding the masses as follows

$$ \boldsymbol{\tau} = \sum_{j=1}^{3} m_j \delta \mathbf{r}_{M\to m_j} \times \mathbf{g}^S \tag{18} $$

$\delta \mathbf{r}_{M\to m_j}$ is designed from the theoretical torque $\boldsymbol{\tau}$ [1] by using Eq. (18). However, because the matrix $\mathbf{g}^S$ is always non-invertible, $\boldsymbol{\tau}$ can be mapped to $\delta \mathbf{r}_{M\to m_j}$ as

$$ \delta \mathbf{r}_{M\to m_j} = \frac{\mathbf{g}^S \times \boldsymbol{\tau}}{m_j \|\mathbf{g}^S\|^2} \tag{19} $$

This control torque can compensate for the offset in the directions perpendicular to

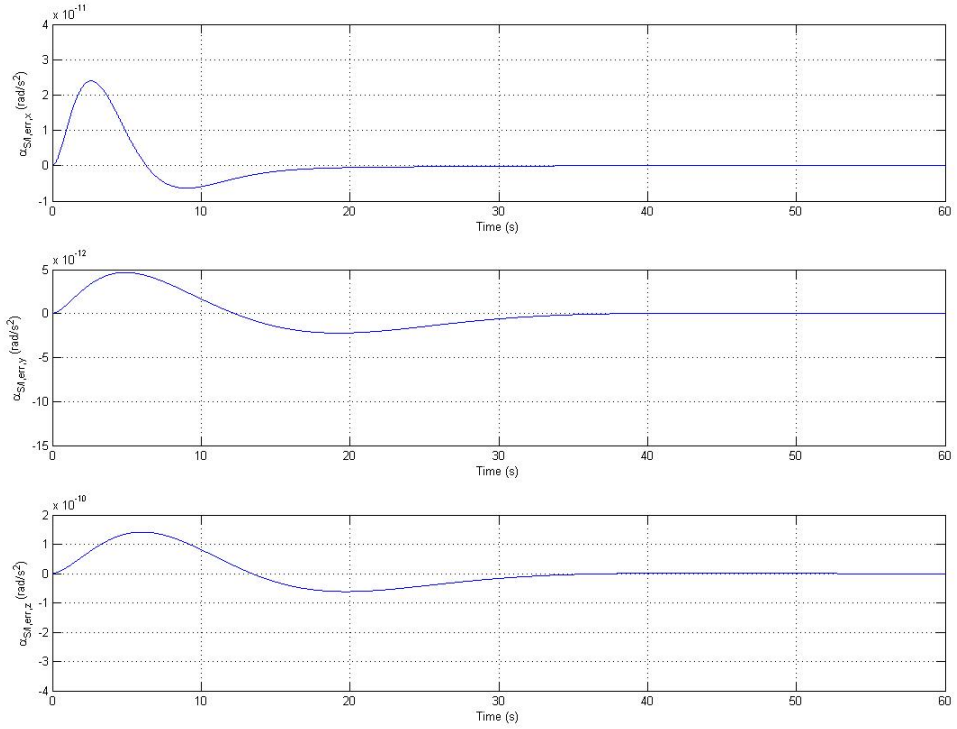

Figure 5: Angular acceleration error from system dynamics

the gravity field, but not in the direction parallel to the gravity. Therefore, Eq. (19) can be substituted into Eq. (18) by noting that $\mathbf{g}^S \cdot \boldsymbol{\tau} = 0$. Then,

$$-m_j \left(\frac{\mathbf{g}^S \times \mathbf{g}^S \times \boldsymbol{\tau}}{m_j \|\mathbf{g}^S\|^2} \right) = - \left(\frac{(\mathbf{g}^S \cdot \boldsymbol{\tau})\, \mathbf{g}^S - (\mathbf{g}^S \cdot \mathbf{g}^S)\, \boldsymbol{\tau}}{\|\mathbf{g}^S\|^2} \right) = \boldsymbol{\tau} \tag{20}$$

The control input is designed as the translation of the proof masses ($\delta \mathbf{r}_{M \to m_j} = \mathbf{u}$). The system dynamics combined with quaternion kinematics is presented as the entire balancing model as follows

$$\begin{bmatrix} \dot{\boldsymbol{\omega}}_{S/I} \\ \dot{\mathbf{q}}_{S/I} \\ \delta \mathbf{r}_{M \to m_j} \end{bmatrix} = \begin{bmatrix} {}^{CR}\mathbf{I}_u{}^{-1} \left(-\boldsymbol{\omega}_{S/I} \times {}^{CR}\mathbf{I}_u \boldsymbol{\omega}_{S/I} + \mathbf{r}^S_{CR \to \bullet_s} \times \mathbf{f}_{g,u} + \boldsymbol{\tau} \right) \\ \frac{1}{2} \mathbf{q}_{S/I} \boldsymbol{\omega}^{(q)}_{S/I} \\ \mathbf{u} \end{bmatrix} \tag{21}$$

where $\boldsymbol{\omega}^{(q)}_{S/I} = (0, \boldsymbol{\omega}_{S/I})$ and the control input $\mathbf{u}$ is the position of the proof masses.

The control torque of a PID controller is defined as a function of attitude and

angular velocity errors. The control torque equation is written as

$$\boldsymbol{\tau} = -K_{q}\mathbf{q}_{err}^{(v)} - K_{I}\int_{0}^{\tau}\mathbf{q}_{err}^{(v)}(\tau)d\tau - K_{\omega}\boldsymbol{\omega}_{S/I} \tag{22}$$

where $\mathbf{q}_{err} = [q_1^{err},\ q_2^{err},\ q_3^{err},\ q_4^{err}]$ and $\mathbf{q}_{err}^{(v)} = [q_2^{err},\ q_3^{err},\ q_4^{err}]$. The error quaternion $\mathbf{q}_{err}$ is calculated by multiplying the desired quaternion $\mathbf{q}_{d}$ with the estimated quaternion $\bar{\mathbf{q}}$ [4] as follows

$$\begin{bmatrix} q_1^{err} \\ q_2^{err} \\ q_3^{err} \\ q_4^{err} \end{bmatrix} = \begin{bmatrix} q_1^{d} & -q_2^{d} & -q_3^{d} & -q_4^{d} \\ q_2^{d} & q_1^{d} & -q_4^{d} & q_3^{d} \\ q_3^{d} & q_4^{d} & q_1^{d} & -q_2^{d} \\ q_4^{d} & -q_3^{d} & q_2^{d} & q_1^{d} \end{bmatrix} \begin{bmatrix} \bar{q}_1 \\ \bar{q}_2 \\ \bar{q}_3 \\ \bar{q}_4 \end{bmatrix} \tag{23}$$

When designing the controller for the balancing system, the reference quaternion is simply given by $\mathbf{q}_{d} = [1,\ 0,\ 0,\ 0]$. The variables K_{q}, K_{I}, and K_{ω} are the proportional, integral, and derivative gains, respectively. The proposed attitude feedback controller utilizes the quaternion and the angular velocity measured by the sensors. Since the balancing system is modeled as a second-order system, the control torque includes the derivative term of the attitude, so that this PID controller will always drive the error to zero.

When the angular velocity and the error quaternion are equal to zero, Eq. (21) becomes

$$\dot{\boldsymbol{\omega}}_{S/I} = {}^{CR}\mathbf{I}_{u}{}^{-1}(\tilde{\mathbf{r}}_{CR\rightarrow\bullet_{u}}^{S} \times m_{u}\mathbf{g}) = 0 \tag{24}$$

where

$$\tilde{\mathbf{r}}_{CR\rightarrow\bullet_{u}}^{S} \times m_{u}\mathbf{g} = \mathbf{r}_{CR\rightarrow\bullet_{s}}^{S} \times \mathbf{f}_{g,u} + \boldsymbol{\tau} \tag{25}$$

The gravity vector has only z component with respect to the body frame since g_{x}^{S} and g_{y}^{S} go to zero. Therefore, Eq. (24) can be written as

$$\begin{bmatrix} I_{11}^{-1} & I_{12}^{-1} & I_{13}^{-1} \\ I_{12}^{-1} & I_{22}^{-1} & I_{23}^{-1} \\ I_{13}^{-1} & I_{23}^{-1} & I_{33}^{-1} \end{bmatrix} \begin{bmatrix} \tilde{r}_{y}\mathrm{g}_{z}^{S} \\ -\tilde{r}_{x}\mathrm{g}_{z}^{S} \\ 0 \end{bmatrix} = \begin{bmatrix} I_{11}^{-1}\tilde{r}_{y}\mathrm{g}_{z}^{S} - I_{12}^{-1}\tilde{r}_{x}\mathrm{g}_{z}^{S} \\ I_{12}^{-1}\tilde{r}_{y}\mathrm{g}_{z}^{S} - I_{22}^{-1}\tilde{r}_{x}\mathrm{g}_{z}^{S} \\ 0 \end{bmatrix} = 0 \tag{26}$$

which yields $\tilde{r}_x = \tilde{r}_y = 0$. This implies that the platform is balanced in x and y directions. But we still have the vertical component of the offset. This component will be estimated using an Extended Kalman filter as presented in the following section.

3.2 Extended Kalman Filter for Vertical Imbalance

Once the offset perpendicular to $\mathbf{g}^S$ is balanced by the controller, the extended Kalman filter(EKF) is used to estimate the vertical offset between the center of rotation and the center of mass [1]. Probably the most widely used estimator for nonlinear systems is the EKF which simply linearizes all the nonlinear models so that the traditional linear Kalman filter equations can be applied. More details about EKF can be shown in Refs. [1, 9, 20].

The state equation of the EKF can be written as

$$\dot{x}(t) = f(x) + \omega(t) \tag{27}$$

where $\omega(t)$ represents the process noise, which is assumed to be a Gaussian white-noise process with mean zero and covariance $Q(t) \in \mathbb{R}^{4\times4}$. If the balancing masses do not move during estimation, the system dynamics from Eq. (13) can be expressed as

$${}^{CR}\mathbf{I}_u \boldsymbol{\alpha}_{S/I} + \boldsymbol{\omega}_{S/I} \times {}^{CR}\mathbf{I}_u \boldsymbol{\omega}_{S/I} = \mathbf{r}_{CR\to\bullet_u} \times \mathbf{f}_{g,u} \tag{28}$$

The state equation is then given by Eq. (28), yielding

$$f(x) = \begin{bmatrix} {}^{CR}\mathbf{I}_u{}^{-1}\left(-\boldsymbol{\omega}_{S/I} \times {}^{CR}\mathbf{I}_u \boldsymbol{\omega}_{S/I} + \mathbf{r}^{off} \times \mathbf{f}_{g,u}\right) \\ 0 \end{bmatrix} \tag{29}$$

where $x = [\boldsymbol{\omega}_{S/I},\ r_z^{off}]$ and $\mathbf{r}^{off} = [0,\ 0,\ r_z^{off}]$, which only has the vertical component of the offset between the center of rotation and the center of mass. Here, the unknown parameter r_z^{off} is augmented into the state with the corresponding dynamics to be $\dot{r}_z^{off} = 0$. The initial mean and covariance of the state are assumed to be known as

$\hat{x}(t_0) = x_0$ and P_0.

In the prediction step, the estimate and the covariance matrix of the state are given by

$$\dot{\hat{x}}(t) \approx f(\hat{x}(t), t) \tag{30}$$

$$P(t) = E\{\delta(t)\delta^T(t)\} \quad \in \mathbb{R}^{4\times 4} \tag{31}$$

where $\hat{x}(t)$ is the minimum covariance estimate of the state and $\delta(t) = x(t) - \hat{x}(t)$ is the state error. The derivative of the state error can be expressed as a linear approximation by using a Taylor series expansion as follows

$$\dot{\delta}(t) = F(t)\delta(t) + w(t), \qquad F(t) = \left.\frac{\partial f(x,t)}{\partial x}\right|_{\hat{x}(t)} \tag{32}$$

and the covariance matrix of the state satisfies the Riccati equation

$$\dot{P}(t) = F(t)P(t) + P(t)F^T(t) + Q(t) \tag{33}$$

In the measurement step, assume that the the angular velocity is taken at time t_k measured by the inertial measurement unit(IMU). The output equation is given by

$$z(t_k) = Hx(t_k) + v(t_k), \quad \text{where} \quad H = \begin{bmatrix} 1 & 0 & 0 & 0 \\ 0 & 1 & 0 & 0 \\ 0 & 0 & 1 & 0 \end{bmatrix} \tag{34}$$

and $v(t)$ represents the measurement noise with covariance $R(t) \in \mathbb{R}^{3\times 3}$. Then the estimate of $x(t_k)$ measured at time t_k is given by

$$\hat{x}^+(t_k) = \hat{x}^-(t_k) + K(t_k)\left[z(t_k) - \hat{z}(t_k)\right], \quad \text{where } \hat{z}(t_k) = H\hat{x}^-(t_k) \text{ and} \tag{35}$$

$$K(t_k) = P^-(t_k)H^T(t_k)\left[H(t_k)P^-(t_k)H^T(t_k) + R(t_k)\right]^{-1} \tag{36}$$

$\hat{x}^-(t_k)$ and $P^-(t_k)$ is the predicted values immediately before the measurement and $\hat{x}^+(t_k)$ and $P^+(t_k)$ is the values after the measurement. The state covariance matrix after the measurement is given by

$$P^+(t_k) = (I - K(t_k)H)P^-(t_k)(I - K(t_k)H)^T + K(t_k)R(t_k)k(t_k)^T \tag{37}$$

In summary, a two-step design is presented to balance the platform in this chapter. The PID control algorithm generates the control torque calculated from Eq. (22) to minimize the offset in x and y directions. Once the offset perpendicular to the gravity is balanced, the offset in z direction is estimated using the Extended Kalman filter and compensated by moving the vertical proof mass according to the estimated value.

CHAPTER IV

SIMULATION AND EXPERIMENTAL RESULTS

4.1 Simulation Results

In this section, the balancing controller and the EKF described above are tested on simulations of the platform of the ASTROS facility. These simulations are implemented using MATLAB/Simulink and it is the exact same control software that will be used in the experiments. The outputs of the Simulink model also drive a virtual-reality environment that provides a relatively realistic 3D visualization of the platform's motion as shown Fig. 6. These simulation results include the PID attitude controller and the EKF for vertical imbalance described in chapter 3. First, the PID controller is tested to stabilize the attitude and the angular velocity. Second, the EKF is tested to estimate the location of the center of mass along z axis.

The angular velocity can be measured by the IMU and the rate-gyros, which are simulated by adding noise, bias, and drift to the true angular velocity [6]. The measurement noises, bias, and drift produced by IMU are $[0.14,\ 0.14,\ 0.14]^T$ deg/s (standard deviation of Additive White Gaussian Noise), $[0,\ 0,\ 0]^T$ deg/s, and $[0,\ 0,\ 0]^T$ deg/s^2, respectively based on the experimental data after being filtered by a 4-th order discrete-time Butterworth filter. The default values for the discrete-time angular velocity measured by the rate-gyro are $[0.05,\ 0.05,\ 0.05]^T$ deg/s (standard deviation of AWGN), $[-0.9,\ 1.1,\ 0.8]^T$ deg/s, and $[1.2e^{-3},\ -2.3e^{-3},\ 1.0e^{-3}]^T$ deg/s^2, respectively.

The $\mathbf{q}_{S/I}$ can be measured by the IMU, VICON system, and the dual-axis inclinometer. The default standard deviation of AWGN added by the IMU is $[0,\ 0,\ 0,\ 0]^T$, and the AWGN standard deviation of the VICON system $[7e^{-5},\ 7e^{-5},\ 7e^{-5},\ 7e^{-5}]^T$, based on experimental data. The dual-axis inclinometer is newly installed for the

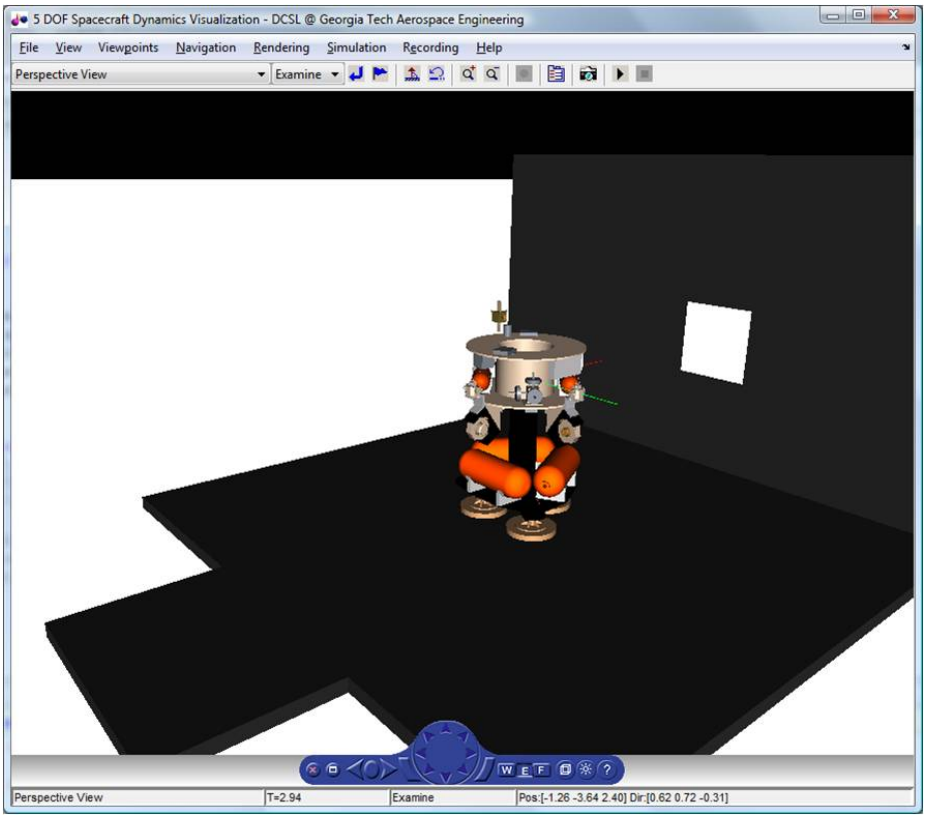

Figure 6: The 3D visualization of the platform

balancing system that shows more accurate data from the experiments. Therefore, the standard deviation of the AWGN added by the inclinometer can be ignored.

The mass moment of inertia matrix, the center of gravity vector and other parameters used for the simulation are estimated [8] as shown below.

$$m_s = 134 \text{ kg},\ m_1 = 2.853 \text{ kg},\ m_2 = 1.962 \text{ kg},\ m_3 = 1.045 \text{ kg}$$

$$^{CR}\mathbf{I}_u = \begin{bmatrix} 20.2012 & -0.0899 & -0.0469 \\ -0.0899 & 12.9943 & -0.4187 \\ -0.0469 & -0.4187 & 16.2764 \end{bmatrix} (\text{kgm}^2),\ \mathbf{r}_{CR\to\bullet_u} = \begin{bmatrix} -5\times10^{-6} \\ 5\times10^{-6} \\ -3\times10^{-4} \end{bmatrix} (\text{m}) \tag{38}$$

where m_s is the mass of the upper stage and m_1, m_2, and m_3 are the loads of three linear stages, which are the same weights as what used in the experiments. The initial states are given by $\boldsymbol{\omega}_{S/I}(0) = [0,\ 0,\ 0]^T$ rad/s, $\phi_{S/I}(0) = 1\,\text{deg}$, and $\theta_{S/I}(0) = 1$, where $\phi_{S/I}$ is the roll angle and $\theta_{S/I}$ is the pitch angle. The yaw angle is not considered for

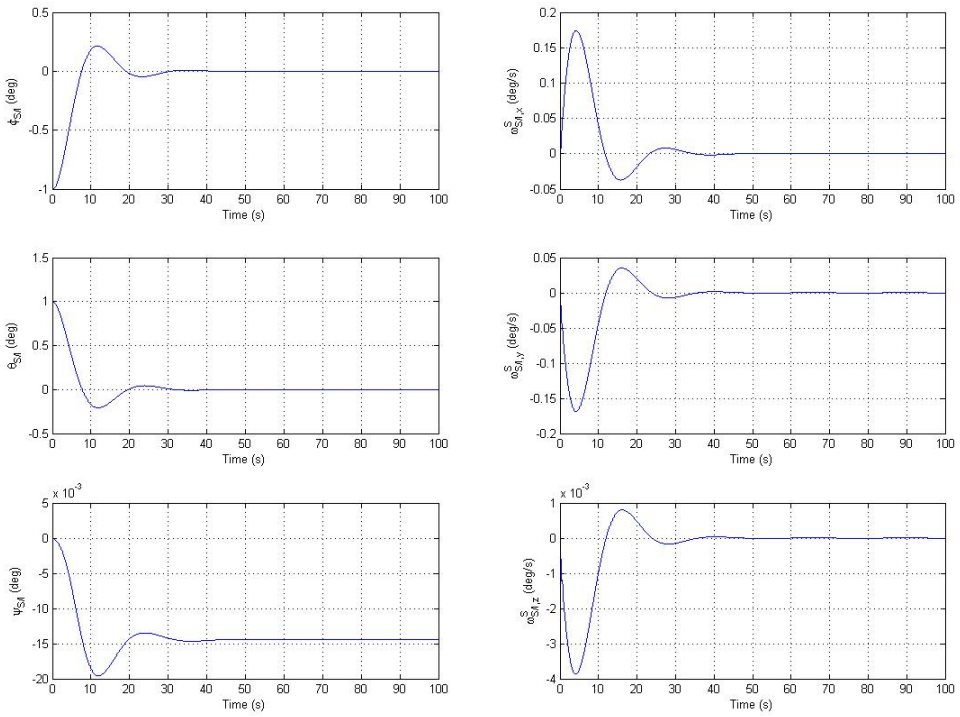

Figure 7: Euler angles and angular velocity expressed in the body frame

the balancing procedure. The control gains are chosen to be $K_\omega = 5$, $K_q = 1$, and $K_I = 1$.

4.1.1 PID Controller

An initial simulation was run in order to validate the automatic mass balancing technique. An offset and other values are simulated with values shown in Eq. (38). An initial angular velocity is assumed to be zero. The simulation result was demonstrated in Figs. 7-8. Fig. 7 shows the convergence of Euler angles and the angular velocity of the upper stage with respect to the inertial frame. Applying the control law given in Section 3.1, we observe that the attitude and the angular velocity go to zero.

As shown as in Fig. 8, the offsets in x and y directions converge to zero, but the proposed adaptive controller cannot balance the offset along z direction. The final positions of the balance masses are $\delta r_{m_1} = 2.3341 \times 10^{-4}$ m and $\delta r_{m_2} = -3.3828 \times 10^{-4}$ m.

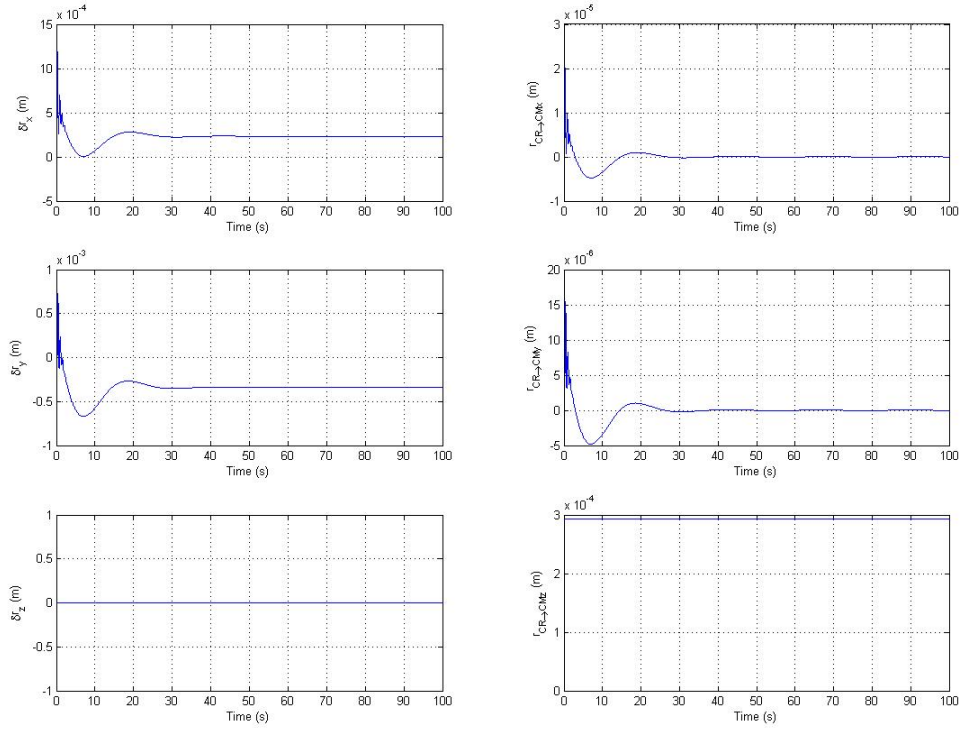

Figure 8: Balance masses' position and convergence of the estimated offsets

These simulation results agree with our analysis presented in preceding sections.

4.1.2 EKF for vertical Imbalance Compensation

In this section, the unbalanced vertical offset is estimated using the Extended Kalman filter as explained in section 3.2. For this simulation, the EKF was fed angular velocity measurements from the IMU and process and measurement covariance matrices have been chosen as

$$\mathbf{Q} = E(\omega\omega^T) = diag(10^{-6},\ 10^{-6},\ 10^{-6},\ 10^{-10})\ [rad^2/s^4, rad^2/s^4, rad^2/s^4, m^2] \tag{39}$$

$$\mathbf{R} = E(vv^T) = diag(2.5 \times 10^{-6},\ 2.5 \times 10^{-6},\ 2.5 \times 10^{-6})\ [rad^2/s^2] \tag{40}$$

and the initial error covariance matrix $\mathbf{P}_0$ is given by

$$\mathbf{P}_0 = diag(10^{-9},\ 10^{-9},\ 10^{-9},\ 10^{-6})\ [rad^2/s^2, rad^2/s^2, rad^2/s^2, m^2] \tag{41}$$

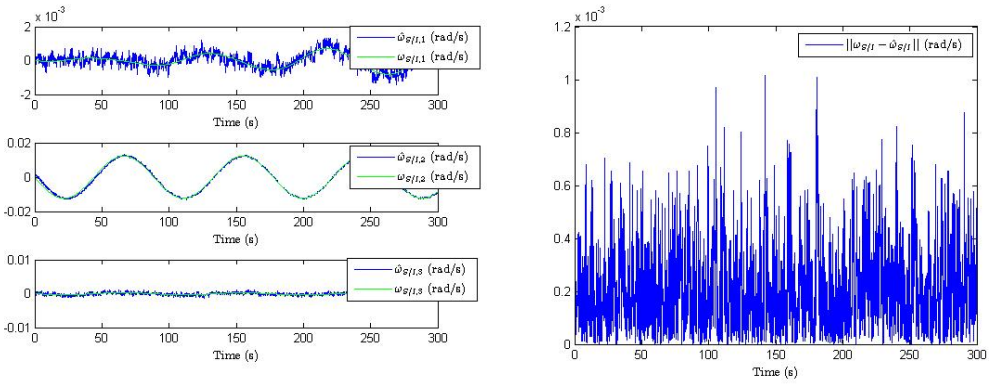

Figure 9: Estimated and true angular velocity and the estimation error

To estimate the states, an initial pitch angle is given by 10 deg and the corresponding quaternion is $\mathbf{q}_0 = [0.9962\ 0\ 0.0872\ 0]$ to start with an non-zero angular velocity. An offset is simulated with initial value $\mathbf{r}^{off}(0) = [0\ 0\ 0]$ (m) and the initial angular velocity $\boldsymbol{\omega}_{S/I}(0) = [0\ 0\ 0]$ (rad/s).

The estimate of the angular velocity and the estimation error obtained with the EKF are plotted in Fig. 9. The angular velocity error is less than 10^{-3} rad/s. Fig. 10 shows the estimated value of the vertical offset and its estimation error. The average estimate after 200 sec is 4.461×10^{-5} (m), which converges to the initial value (4.959×10^{-5}). After r_z^{off} has been estimated, the balance mass m_z can be moved along the z axis to balance the last direction. Therefore, the offset in all three directions can be eventually balanced.

4.2 Experimental Results

To test an automatic balancing system, the 5-DOF experimental platform of the ASTROS facility uses three linear actuators with a dual-axis inclinometer. The chosen linear stages are from the MSL-25-14 from Newmark Systems Inc [25] as shown in Fig. 11.

In order to precisely move the balance masses, the three linear stages slide up to 50 mm along their axis, respectively. They have ball screws to move 2.54 mm for each

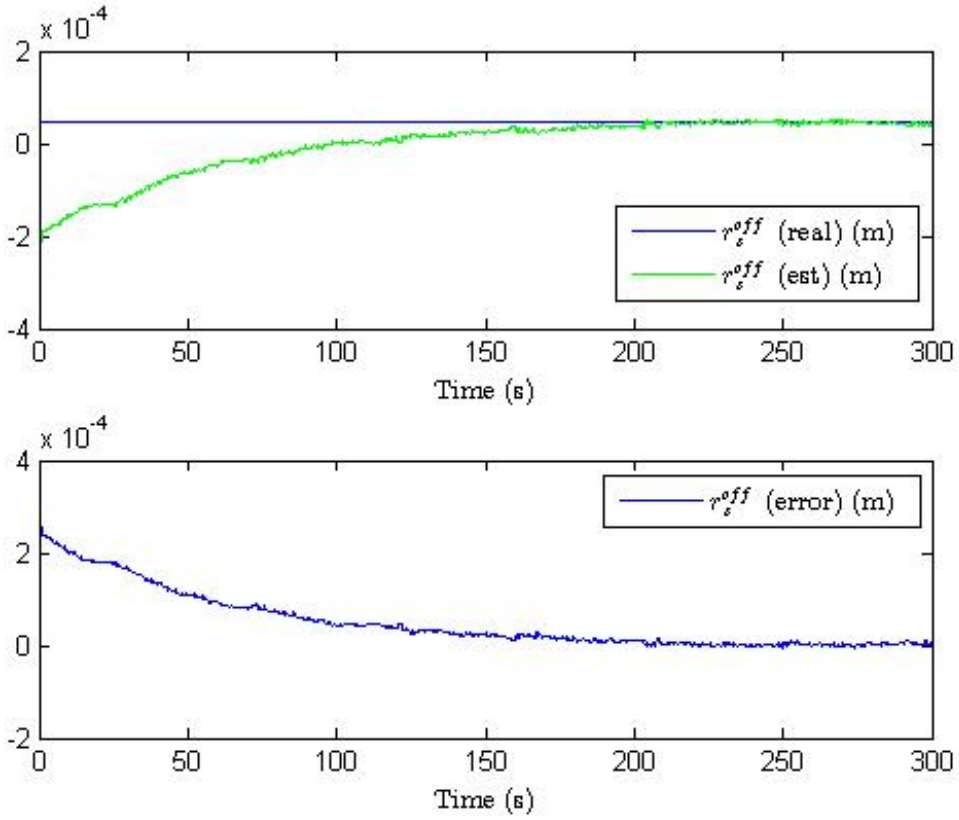

Figure 10: Estimated and true offset and the estimation error

revolution. Each stage comes with a MDrive intelligent stepper motor, which is integrated with a high resolution microstepping driver and a full featured programmable motion controller. This motor rotates 1.8° per step or 200 steps per revolution. The microstep resolution selection divides the number of steps to yield a finer resolution. The default value of the microstep resolution is 256, which yields 51200 microsteps per revolution. The actuators can move at a top speed of 5,000,000 microsteps/sec and a top acceleration of 1.5×10^9 microsteps/sec². To program the actuator, an initial (VI) and a maximum velocity (VM) as well as the required distance are needed to calculate the actual time as shown in Fig. 12. The position resolution is 2048 microsteps, the velocity resolution is 0.5961 microsteps/sec, and the acceleration resolution is 90.9 microsteps/sec². Table. 1 shows the specifications of the linear stage combined with the stepper motor.

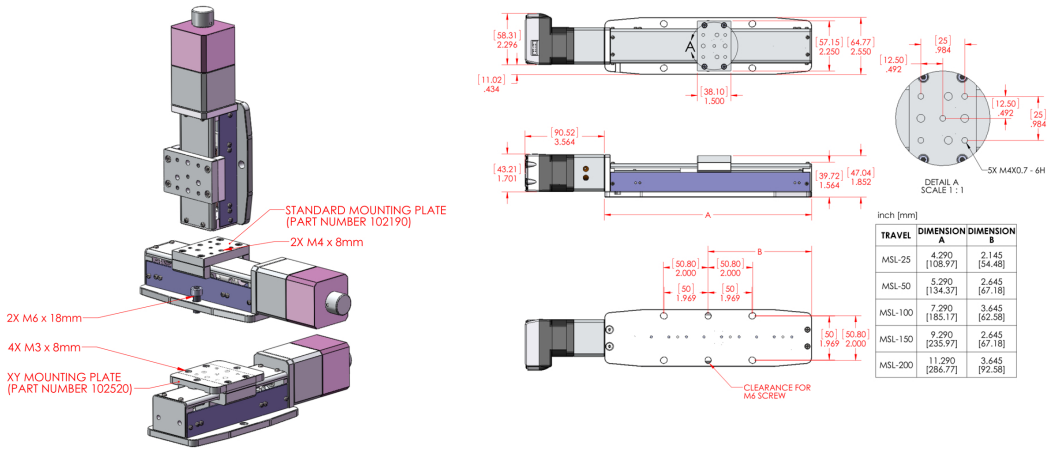

Figure 11: Overview of the three-axis linear actuator and its dimensions

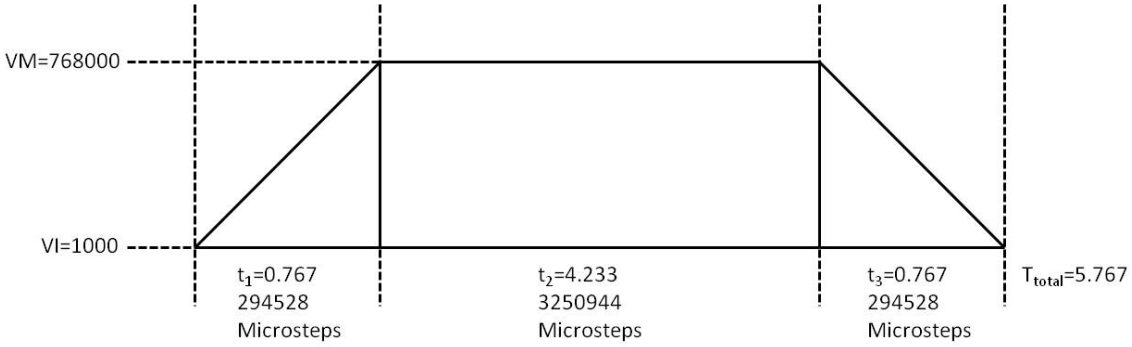

Figure 12: Trapezoidal move profile

Fig. 13 shows the balancing system installed on the upper stage. The system has 1.063 kg mass only on the vertical stage. Therefore, the stage on the bottom has the weights of the two stages plus the proof mass and the middle stage has the weights of the vertical stage plus the proof mass as shown in Eq. 38. The system operates in a party mode in order to control three stages at the same time.

Instead of other sensors [23], a dual axis inclinometer is installed for the balancing system in order to deliver better accuracy. The inclinometer (Solar-2-30-1) from Level Developments Ltd. provides 30° range and 0.001° resolution [26]. The roll and pitch angles are measured from the inclinometer at 20 Hz. Fig. 14 shows the raw data of the angles measured by IMU, VICON, and the inclinometer. The misalignment between

Table 1: Specifications of the linear actuator

Specification	Value	Specification	Value
Travel Length	$50\,mm$	Motor Type	Stepper
Resolution	$0.04\,\mu m$	Input Voltage	+12-48 VDC
Accuracy	$0.6\,\mu m$	Communication	RS-422/485
Max. Speed	$25\,mm/sec$	Steps/Rev	51200
Max. Load	$4.5\,kg/each$	Velocity Range	$\pm 25\,mm/sec$
Stage Weight	$0.73\,kg$	Motor Weight	$0.29\,kg$

the sensors is up to 1.2 deg that can cause an error of the control system.

The automatic balancing system is installed on the upper stage of the platform and both the actuator and the inclinometer communicate to an on-board computer using the RS-232 protocol. Three stages of the actuator are daisy chained and controlled independently by assigning a device name to each stage and enabling the party mode. The on-board computer runs Mathworks' xPC Target real-time environment to collect sensor data and implement control algorithms for the actuator. In this environment a host comuputer with MATLAB/Siumulink creates control models using Simulink blocks for xPC Target. A Wi-Fi router provides wireless communication between the target and the host computer. All on-board electronics are powered by two rechargeable lithium-iron batteries [23]. The schematic of the overall connections to the computer are shown in Fig. 15.

The PID controller using the quaternion and angular velocity feedback was implemented on the ASTROS facility. In the experiment, the angular velocity and the roll and pitch angles of the upper stage with respect to the inertial frame were measured with the inclinometer at 20 Hz. The experiment was carried out on the balancing model presented in Section. 3.1. The control gains were set as $K_{\omega} = 5$, $K_{q} = 1$,

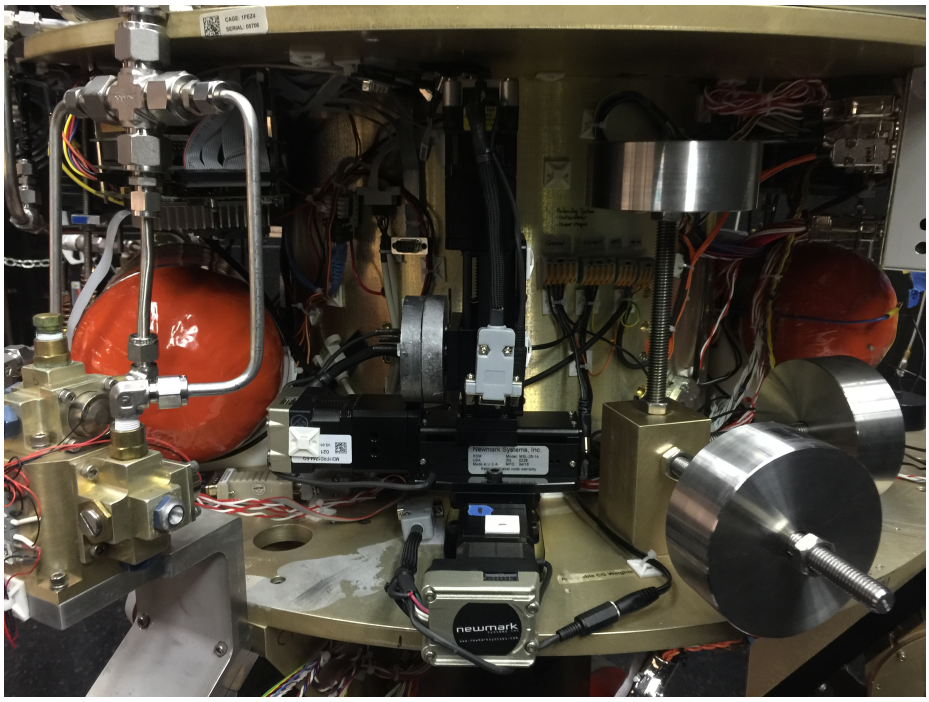

Figure 13: Balancing system installed on the upper stage

$K_I = 1$ which were tuned from the simulation. At the beginning of the experiment, an initial angular velocity of $\boldsymbol{\omega}_0 = [0.06,\ 0,\ 0]\,\mathrm{deg/s}$, an roll angle $\phi_0 = -1.61\,\mathrm{deg}$, and an pitch angle $\theta_0 = -2.93\,\mathrm{deg}$ were applied. Fig. 16 shows the trajectories of the angles and the angular velocities. After 120 sec, the roll and pitch angles converged to zero while the angular velocity was stabilized. This behavior agreed with the simulation result as expected, but the platform was not perfectly balanced. It is attributed to the limitation of accuracy of the inclinometer. As shown in Fig. 17, the linear stages slided -1.1 mm and 1.5 mm along x and y axes during the balancing procedure.

After the balancing experiment, the offset between the center of mass and the center of rotation was compensated in two directions, which implies the center of mass became parallel to the gravity.

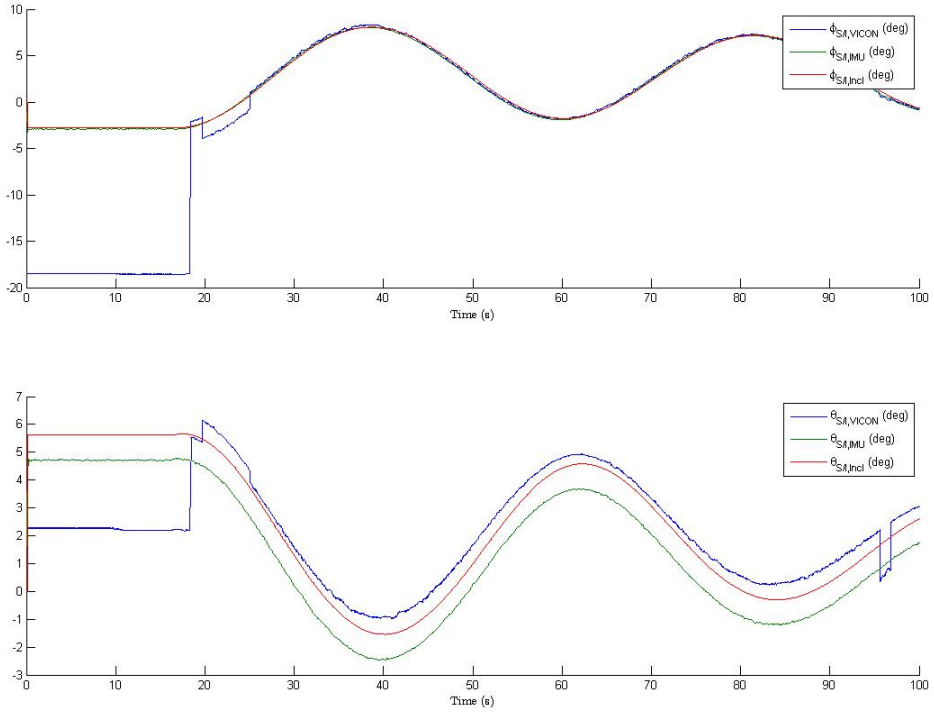

Figure 14: Comparison of the roll and pitch angles between the sensors

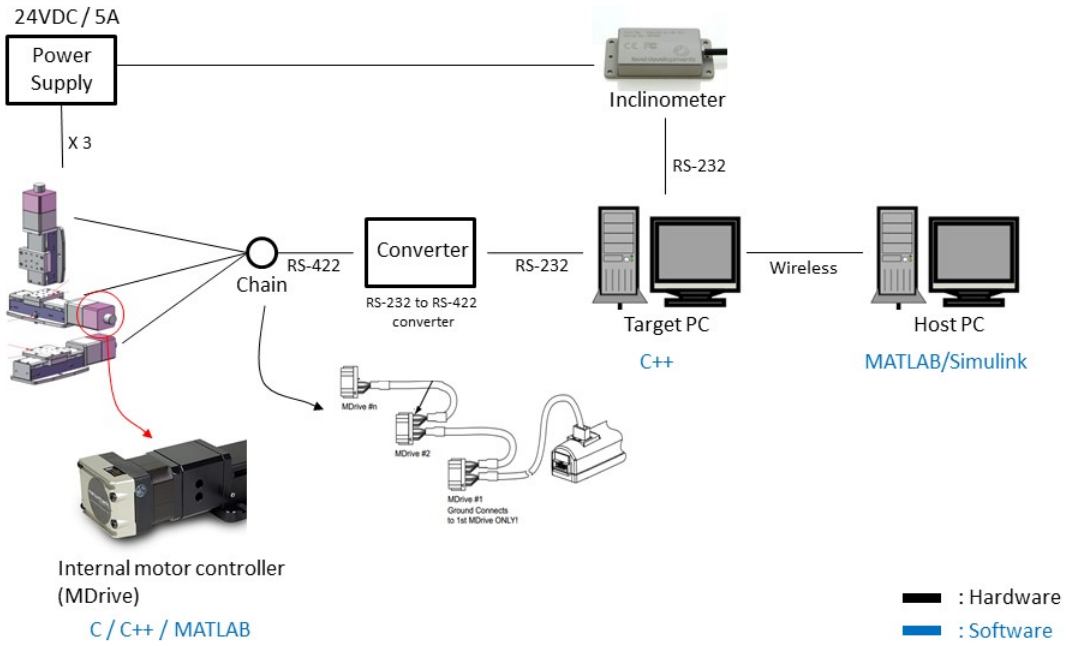

Figure 15: Overall Schematic of the balancing system in reference to the connection to the computer

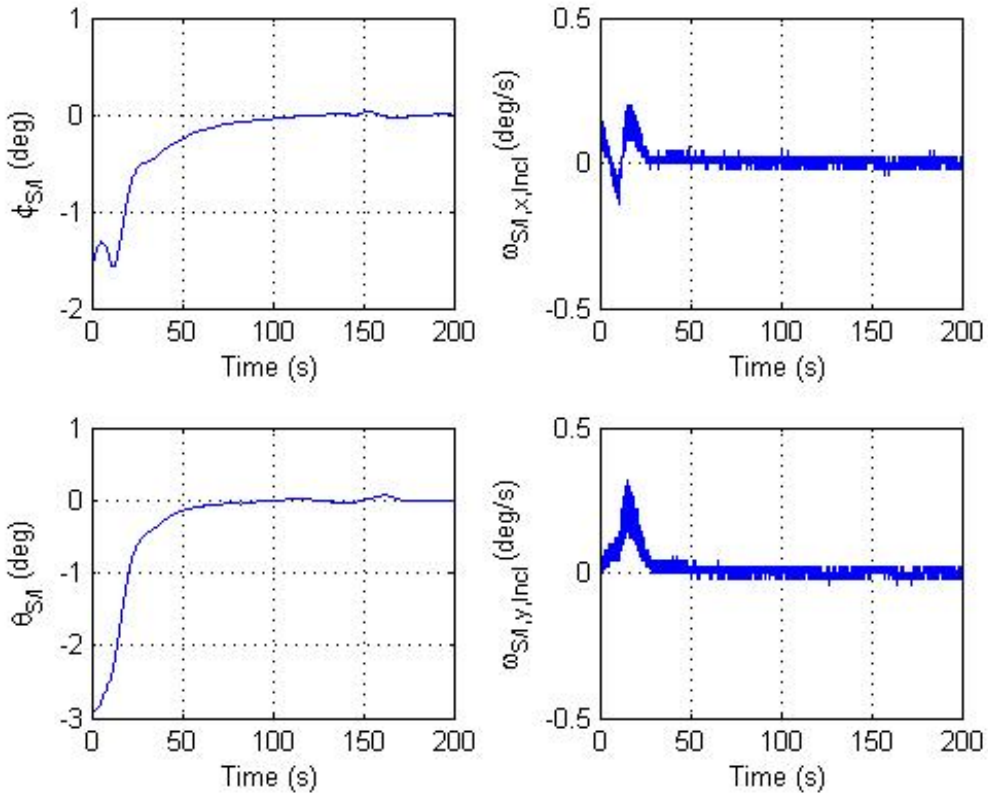

Figure 16: Euler angles and angular velocity expressed in the body frame

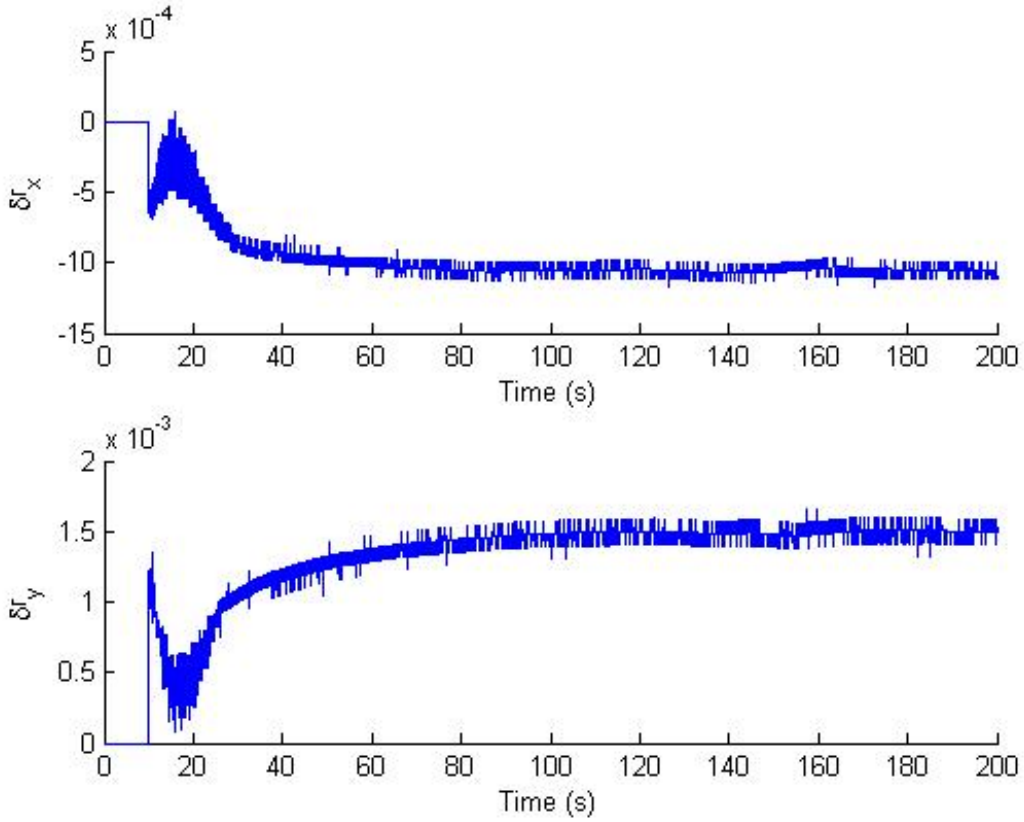

Figure 17: Balance masses' position

CHAPTER V

CONCLUSIONS

5.1 Summary

In this thesis, an automatic balancing system has been developed to minimize the gravitational torque acting on the spacecraft simulator. The proposed balancing system can eliminate the offset using only sliding masses. However, the control torque generated by the linear actuators is constrained in the direction perpendicular to the gravity. To overcome this physical limitation of the linear stages, a two-step design has been proposed. First, a quaternion based PID controller has been presented. This dual-axis controller is one of the simplest form for the attitude control which is applied directly to the quaternion error. The simulation and experimental results proved the stabilization of the attitude and the angular velocity. Once the offsets in x and y axes are compensated, the vertical offset is estimated using an Extended Kalman Filter. The main contribution of this work is that the automatic balancing system greatly reduce time and labor and accurately minimize the disturbance torque acting on the platform compared with the manual balancing system.

5.2 Future Work

Apart from the theoretical techniques developed in this research, here are some further attempts to improve the accuracy of the system and to take into consideration the reality.

- The attitude measurements of the sensors installed on the platform need to be aligned with each other for future experiments.
- For the second step of the balancing procedure, the EKF proposed in Section

3.2 needs to be tested to estimate the vertical offset in the real system.

REFERENCES

[1] CHESI, S., GONG, Q., PELLEGRINI, V., CRISTI, R., and ROMANO, M., "Automatic mass balancing of a spacecraft three-axis simulator: Analysis and experimentation," in *Journal of Guidance, Control, and Dynamics,* vol. 37, pp. 197-206, January-February 2014.

[2] CHO, D.-M., JUNG, D., and TSIOTRAS, P., "A 5-DOF experimental platform for spacecraft rendezvous and docking," in *AIAA Infotech, @ Aerospace Conference,* (Seattle, WA), April 6-9 2009. AIAA Paper 2009-1869.

[3] CRASSIDIS, J. L., MARKLEY, F. L., and CHENG, Y., "Survey of nonlinear attitude estimation methods," *Journal of Guidance, Control, and Dynamics,* vol. 30, pp. 12–28, January-February 2007.

[4] FRESK, EMIL and NIKOLAKOPOULOS, George, "Full Quaternion Based Attitude Control for a Quadrotor," in *2013 European Control Conference,* (Switzerland), July 17-19 2013.

[5] FULLMER, R. R., "Dynamic ground testing of the skipper attitude control system," *34th AIAA Aerospace Science Meeting and Exhibit,* AIAA Paper 1996-0103, January 15-18 1996.

[6] FILIPE, N., "Nonlinear Pose Control and Estimation for Space Proximity Operations: an Approach Based on Dual Quaternions," Ph.D Dissertation, Georgia Institute of Technology, (Atlanta, GA), December 2014.

[7] HATCHER, N. M., and YOUNG, R. N., "An automatic balancing system for use on frictionlessly supported attitude-controlled test platforms," NASATN D-4426, Langley Research Center, March 1968.

[8] JUNG, D. and TSIOTRAS, P., "A 3-DOF experimental test-bed for integrated attitude dynamics and control research," *AIAA Guidance, Navigation, and Control Conference,* (Austin, TX), 2003, AIAA 2003-5331.

[9] JULIER, J., and Uhlmann, J. K., "A new extension of the Kalman filter to nonlinear systems," *Signal Processing, Sensor Fusion, and Target Recognition VI,* Vol. 3068, 1997, pp. 182-193.

[10] KIM, J. and AGRAWAL, B., "Automatic mass balancing of air-bearing-based three-axis rotational spacecraft simulator," in *Journal of Guidance, Control, and Dynamics,* vol. 32, May-June 2009.

[11] KEIM, J. A., ACIKMESE, A. B., and SHIELDS, J. F., "Spacecraft inertia estimation via constrained least squares," *IEEE Aerospace Conference,* IEEE, (Piscataway, NJ), 4–11 March 2006.

[12] LEFFERTS, E., MARKLEY, F., and SHUSTER, M., "Kalman filtering for spacecraft attitude estimation," *Journal of Guidance, Control, and Dynamics,* vol. 5, pp. 417–429, September-October 1982.

[13] LEINE, R. I., and WOUW, N., "Stability and convergence of mechanical systems with unilateral constraints" Springer, New York, 2008, pp. 145-148.

[14] MEISSNER, D. M., "A three degrees of freedom test bed for nanosatellite and cubesat attitude dynamics, determination, and control." MS thesis, Naval Postgraduate School, (Monterey, CA) December 2009.

[15] PECK, M. A., MILLER, L., CAVENDER, A. R., GONZALEZ, M., and HINTZ, T., "An airbearing-Based testbed for momentum control systems and spacecraft line of sight," *13th Annual AAS/AIAA Spaceflight Mechanics Meeting,* American Astronautical Society Paper 03-127, February 2003.

[16] PRADO, J., BISIACCHI, G., REYES, L., VICENTA, E., CONTRERAS, F., MESINAS, M., and JUAREZ, A., "Three-axis air-bearing based platform for small satellite attitude determination and control simulation," *Journal of Applied Research and Technology,* Vol. 3, No. 3, December 2005, pp. 222–237.

[17] SCHWARTS, J. L., "The distributed spacecraft attitude control systems simulator: From design concept to decentralized control," Ph.D Dissertation, Virginia Polytechnic Institute and State University, (Blacksburg, VA), July 7 2004.

[18] SCHWARTZ, J. L., and HALL, C. D., "System identification of a spherical airbearing spacecraft simulator," AAS Paper 2004-122, 8–12 February 2004.

[19] SCHWARTZ, J. L., PECK, M. A., and Hall, C. D., "Historical review of airbearing spacecraft simulators," *Journal of Guidance, Control, and Dynamics,* Vol. 26, No. 4, 2003, pp. 513–522.

[20] SIMON, D., "Optimal state estimation" John Wiley & Sons, Inc, New Jersey, 2006.

[21] SMITH, G. A., "Dynamic simulators for test of space vehicle attitude control system," *Proceedings of the Conference on the Role of Simulation in Space Technology, Part C,* Virginia Polytechnic Institute and State University, (Blacksburg, VA), August 20-22 1964, pp. 15-1–15-30.

[22] TANYGIN, S. and WILLIAMS, T., "Mass property estimation using coasting maneuvers," *Journal of Guidance, Control, and Dynamics,* Vol. 20, No. 4, July–August 1997, pp. 625–632.

[23] TSIOTRAS, P., "ASTROS: A 5DOF experimental facility for research in space proximity operations," in *AAS Guidance and Control Conference,* no. 2014-114, (Breckenridge, CO), January 31 - February 5 2014.

[24] YOUNG, J. S., "Development of an automatic balancing system for a small satellite attitude control simulator (SSACS)," M.S. Thesis, Utah State University, (Logan, UT), 1998.

[25] 'MSL Series Linear Stage" Retrieved from http://www.newmarksystems.com/linear-positioners/msl-series/, June 2016.

[26] 'SOLAR-2-30-1-RS232-Dual Axis Inclinometer" Retrieved from https://www.leveldevelopments.com/products/inclinometers/inclinometer-sensors/solar-2-30-1-rs232-dual-axis-inclinometer-30-rs232-interface/, June 2016.